Tribology International 156 (2021) 106802

Contents lists available at ScienceDirect

Tribology International

journal homepage: http://www.elsevier.com/locate/triboint

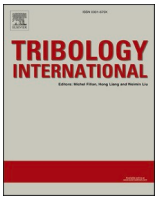

Adhesion modelling by finite elements of three-dimensional fretting

Huaidong Yang *, Itzhak Green

W. Woodruff School of Mechanical Engineering, Georgia Institute of Technology, Atlanta, GA, 30332-0405, USA

ARTICLE INFO

Keywords:
Adhesion
Finite element analysis
Contact mechanics
Fretting

ABSTRACT

This work builds a comprehensive adhesion model by finite elements (FEA) for a deformable hemisphere subject to fretting. The hemisphere is constrained between two rigid and frictionless plates as it is loaded in the normal direction and followed by prescribe oscillatory tangential motions. The material for the deformable hemisphere is gold (Au). The normal direction adhesion contact is based on the classic JKR model; however, the tangential resistance is based on the definition of the shear strength and the surface free energy. That is manifested into interfacial bilinear springs where detachment or reattachment of the two contacting surfaces occur when the springs "break" or "snap-back" at the interface. It is shown that the breakage of the springs may be gradual or avalanching. The tangential resistance effect is robust, that is, it is not influenced by the choice of meshing or the spring settings. When the two surfaces are about to detach, the most part of the contact region deforms plastically. At small fretting amplitudes (with no springs breakage), the fretting loop behaves similarly to that of full stick conditions. Hence, the von-Mises stress distributions, plastic strain distributions, and fretting loops, are similar to those of full stick condition. However, the current adhesion model is structurally less stiff because of the bilinear spring. Conversely, at a large oscillation amplitude, the fretting loop exhibits large energy losses, and yet it does not resemble those of gross slip conditions.

1. Introduction

Friction is a complex phenomenon that is influenced by various effects such as contamination, elastic and plastic deformations, roughness, and adhesion, among others [1]. Emphasis here is placed on adhesion and fretting and the study is particular to the combination of these two effects together. The first work that relates adhesion to friction can possibly be traced back to Desaguliers in 18th century [2]. An adhesion model is developed by Bowden and Tabor, who propose the "plastic junction" concept, which means that adhesion can exhibit tangential resistance by forming a plastic junction at interface [3]. The study in the current work focuses on the modeling of such a tangential resistance by employing interfacial bilinear springs to represent the adhesion effect between metallic contacts, while all that is under fretting conditions. Adhesion is the only physical bond between the surfaces, where an arbitrary "coefficient of friction" is never imposed in the model.

The study of metal-to-metal adhesion can be traced back to 1963 to the work by Keller [4]. When two metallic surfaces are brought to be close enough, the atomic level attractive force can increase significantly, which encapsulates the adhesion effect. Metallic adhesion can influence the process of friction [5], wear [6], and fatigue [7] when the contact is considered microscopically.

Johnson, Kendall, and Robert add the adhesion effect to the Hertzian contact solution in the normal direction in their venerable JKR model [8]. It is based on the balance between the stored elastic energy and the loss of surface energy. The limitation of that model is that adhesion is assumed active only inside the area of contact. An alternative adhesion model, the DMT model, was later developed by Derjaguin, Muller, and Toporov [9]. The DMT model includes the adhesion effect both inside and outside of the area of contact. However, the JKR and DMT models are at odds with each other. Tabor [10], and later Maugis [11] solve this contradiction by showing that JKR model applies for large and compliant contacting bodies while DMT model applies for stiff contacting bodies. They develop, respectively, the Tabor or Maugis parameters to determine whether a contact is more suitable for the JKR or the DMT model. Later, a numerical model based on these two classic adhesion models is incorporated in a finite element analysis (FEA) software to study the loading and unloading behavior of the adhesion in normal contact [12]. Du et al. include plasticity in the loading-unloading adhesion model [13]. However, in all of the above studies, adhesion is considered only in the normal direction. In other words, the models do not consider a tangential direction strength.

Adhesion has been observed experimentally to be related to friction

* Corresponding author.
E-mail addresses: yanghuaidong@gatech.edu (H. Yang), green@gatech.edu (I. Green).

https://doi.org/10.1016/j.triboint.2020.106802
Received 11 September 2020; Received in revised form 4 November 2020; Accepted 24 November 2020
Available online 1 December 2020

Nomenclature

contact radius	
E	elastic modulus
E′	equivalent elastic modulus
k	spring stiffness
l	elongation of the spring
l_c	elongation limitation of the spring
N	total number of springs at the interface
$P_{adhesion}$	pressure distribution due to adhesion effect
$P_{Hertzian}$	pressure distribution due to Hertzian contact
f_c	the tangential force one spring holds at its elongation limitation
F	external normal force (in the positive Y direction)
F_c	pulled-off force in JKR model
F_x	tangential force
r	distance to the center of the contact
R	radius of sphere
S_y	yield strength
S_{sy}	shear strength
ε_p	equivalent plastic strain
δ	nominal tangential displacement
μ	coefficient of friction
ν	Poisson ratio
σ_e	equivalent von-Mises stress
γ	surface free energy
ΔA	contact area of one mesh element
Δγ	adhesion energy

[14]. According to Bowden and Tabor [3], the friction force is proposed to be directly proportional to the contact area and the shear strength of the material. In order to understand the mechanism of contact behavior in the microscopic level, the atomic force microscopic (AFM) was developed in 1986 by Binning et al. [15]. Since then, the AFM has regularly been used to test the relationship between the friction force and the contact area microscopically [16–18]. The contact areas based on the JKR, DMT, or the Maugis models are found to be proportional to the friction force obtained in the AFM experiment. However, theoretical and numerical works of combing sliding friction and adhesion are scarce.

Theoretical and numerical works that do consider friction as an effect of adhesion are those by Johnson [2] and Popov et al. [19]. The theoretical model built by Johnson [2] is based on fracture mechanics, which is complicated to be implemented in numerical simulations. Only some preliminary elastic results are generated in that work. The model built by Popov et al. [19] is based on the method of dimensionality reduction. It studies the contact between a rigid sphere and an elastic flat surface. Linear elastic springs are used to generate tangential resistance effect caused by adhesion. They use the surface energy and shear modulus to define the elastic spring stiffness and maximum elongation of the springs. But the tangential resistance can only be generated for rotational motion since the model is axisymmetric. Moreover, if the model is extended to three dimensions, an issue arises where the results change with the size of the mesh at the interface.

The model in this work is developed to investigate the adhesion effects between a deformable hemisphere and a rigid flat surface under fretting conditions. The material for the deformable body is gold (that is commonly used in electrical contacts). The adhesion effect is considered to generate force and traction in the normal and tangential directions. The normal direction adhesion is based on the classic JKR model, while the tangential resistant traction is generated by applying tuned bilinear elastic springs (defined later) at the interface. An effective "friction" emerges via a hysteretic loop as generated by the adhesion effect combined with an oscillatory tangential loading. The model is robust and insensitive to the mesh settings in the FEA. The results include the distribution of von-Mises stress, plastic strains, and the tangential traction. Only pure adhesion effects are applicable at the interface where no other contrived conditions (e.g., "sticking," or a "coefficient of friction") are ever artificially imposed. Also, the emphasis here is on building the model and methodology. While results are indeed presented for a specific material and an application (electric contact), because of the extreme simulation run times, an exhaustive parametric study is not undertaken (that may be left for a future study). Also, wear is currently excluded (but aspects of such modeling can be found in Ref. [20]).

2. Model

As shown in Fig. 1, the fretting arrangement in this work is for a non-conforming contact between a hemisphere and a rigid flat block. The coordinate system X-Y-Z is shown in Fig. 1, where the origin is located at the center contact point at the bottom of the hemisphere. The mechanical model is symmetric with respect to the X–Y plane. Hence, to reduce the computational effort, the model is simplified to a quarter sphere pressed against a rigid flat block. Adhesion has effects in both the normal and tangential directions. The Tabor parameter [10] is calculated based on the parameters given in Table 1, $\mu_T = [(R\gamma^2)/(E'^2 z_0^3)]^{1/3} = 26$. The Tabor parameter is much larger than 1, which indicates the contact condition is more readily suitable for JKR model rather than the DMT model. Thus, in the normal direction, adhesion is based on the JKR model [8]. In the tangential direction, the resistance traction is based on the maximum shear stress theory and the surface free energy. The interface between the hemisphere and the rigid bottom block is set to be frictionless. However, due to the presence of the adhesion effect in tangential direction, tangential traction is generated during the transverse fretting motions.

The loading condition is force-controlled in the Y direction, and displacement-controlled in the X direction. In order to keep a uniform vertical displacement at the top surface of the hemisphere constant, a rigid flat plate is added there. The interface between the top rigid flat plate and the hemisphere is likewise frictionless. An external force, F, is applied at the top surface of the rigid plate. While keeping this external force fixed, a reciprocal horizontal displacement, δ, is applied to the top surface of the hemisphere to simulate the fretting motion. It is important to note that δ is not the displacement at the contacting interface. The hemisphere has stiffness/flexibility, so the displacement at the contact is smaller. The detailed discussion can be found in Ref. [20].

2.1. External force

A reciprocal horizontal displacement, δ, is applied by discrete loading steps at the top of the deformable hemisphere, with a behavior shown in Fig. 2. It takes 40 steps to finish one cycle of the fretting motion. The amplitude of the motion is either 15 or 20 nm. The top surface of the hemisphere starts from the state as shown in Fig. 1, and is designated as position "A" in Fig. 2. Next, the hemisphere is forced to displace to the furthest position in the positive direction of the X-axis, and is recorded as position "B". Then the hemisphere turns back to the original position, and that is recorded as position "C". As it moves further backwards, the hemisphere reaches the furthest point in the negative position of X-axis, which is recorded as position "D". Finally, the hemisphere turns back to the original position, which previously was designated as point "A." That is the start of the next fretting cycle. So, A_1 indicates the beginning of the first cycle, while A_2 indicates the beginning of the second cycle, etc. A more detailed description on the fretting

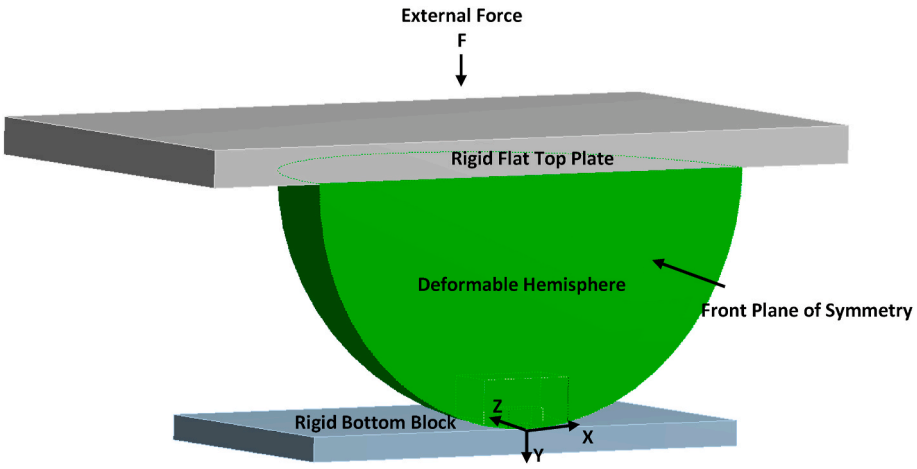

Fig. 1. Fretting model built in ANSYS 17.1.

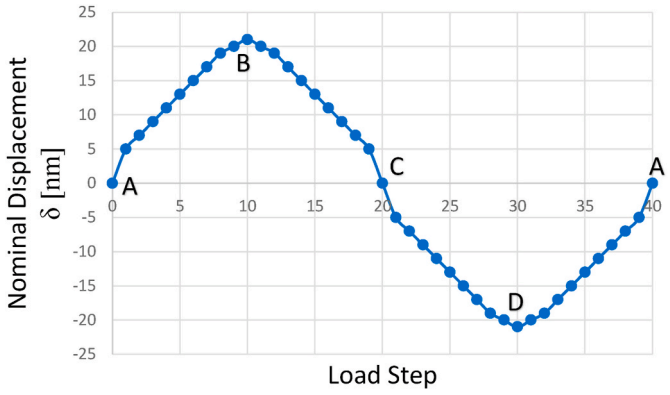

Fig. 2. Loading steps on the top surface of hemisphere for cycle of fretting motion.

model can be found in the work by Yang and Green [21].

According to the JKR model (see Ref. [8]), the external force, F, is related to the other parameters by:

$$F = \frac{4E'a^3}{3R} - \sqrt{8\pi a^3 \Delta\gamma E'} \tag{1}$$

The parameters a and R represent the contact and the hemisphere radii, respectively. The adhesion energy, $\Delta\gamma$, equals to two times of the surface free energy, $\Delta\gamma = 2\gamma$. The equivalent elastic modulus, E', is expressed by:

$$\frac{1}{E'} = \frac{1-\nu_1^2}{E_1} + \frac{1-\nu_2^2}{E_2} \tag{2}$$

where E_1 and E_2 represent the elastic moduli of the two contacting bodies, and ν_1 and ν_2 represent their Poisson ratios. When the surface free energy is of no practical significance, setting $\Delta\gamma = 0$ in Eq. (1) reveals the classical Hertzian solution for a forced normal contact between a hemisphere and a flat. The explicit expression of the contact radius, a, is derived from Eq. (1) to be:

$$a = \left[\frac{3R}{4E'}\left(F + 3\Delta\gamma\pi R + \sqrt{6\Delta\gamma\pi RF + (3\Delta\gamma\pi R)^2}\right)\right]^{\frac{1}{3}} \tag{3}$$

The pressure distribution at the interface is also given by Johnson et al. [2]:

$$p(r) = p_{Hertzian} + p_{adhesion} = \frac{2aE'}{\pi R}\left(1 - \frac{r^2}{a^2}\right)^{\frac{1}{2}} - \sqrt{\frac{2\Delta\gamma E'}{\pi a}}\left(1 - \frac{r^2}{a^2}\right)^{-\frac{1}{2}} \tag{4a}$$

where specifically,

$$p_{adhesion} = -\sqrt{\frac{2\Delta\gamma E'}{\pi a}}\left(1 - \frac{r^2}{a^2}\right)^{-\frac{1}{2}} \tag{4b}$$

The pressure, p(r), consists of a positive Hertzian pressure and a negative adhesion pressure. The positive Hertzian pressure is caused by the elastic deformation of the interface, while the negative adhesion pressure is caused by the adhesion effect in the normal direction.

To include the JKR model in the current finite element model, $p_{adhesion}$ is added in the normal direction nodal-wise. As shown in Fig.3a, a local adhesion force is applied to each node at the bottom surface of the sphere. At a certain input of the external force, F, the contact radius, a, is calculated by Equation (3). For each mesh element, having a central node, i, and coordinates (x_i, y_i), the local radius is $r_i=(x_i^2+ y_i^2)^{1/2}$. By applying that local radius of the node, r_i, the contact radius, a, the material properties, and the geometrical parameters, the negative local adhesion pressure, $P_{adhesion}$, is calculated by Eq. (4b). Thus, the local adhesion force in the normal direction is calculated by the product of local adhesion pressure and the area of the mesh element, ΔA. For each element, there are 9 nodes of the surface in contact; However, the nodal force is only applied to the top left three nodes for the current mesh element as indicated in Fig. 3c. Thus, the local nodal force is $F_i = P_{adhesion}*\Delta A/3$. The other nodes on the element periphery participate in the neighboring elements, and therefore all nodes are eventually accounted for.

The effect of tangential resistance can be achieved by applying bilinear springs in the X-direction. As shown in Fig. 3b, the bilinear spring behaves as a linear spring within the elongation limitation ($-l_c$, l_c), but exerts zero force outside of that range. Principally, the spring "breaks" or "snaps-back" at the limits of $|l_c|$. Therefore, in the model, for each mesh element at the bottom surface of the hemisphere, an interfacial tangential spring is attached. Only elements that are at the contacting interface shall contain bilinear springs; one spring end is linked to a node on the hemisphere, while the other end is linked to an inertial point, i.e., at bottom rigid plate. One spring represents one tangential resisting element. The deactivation of the tangential resistant element is achieved by the "breakage" of the spring (where its internal force "snaps" to zero). The definition of the surface free energy is the energy that is required to create one surface per unit area [22]. Thus, the elastic energy stored in the spring when the spring breaks is equal to the product of the adhesion energy, $\Delta\gamma = 2\gamma$ (where two new surfaces are created), and the area of the contact element,

$$\frac{1}{2}kl_c^2 = \Delta A\Delta\gamma \tag{5}$$

The parameter, k, represents the tuned spring stiffness, and the

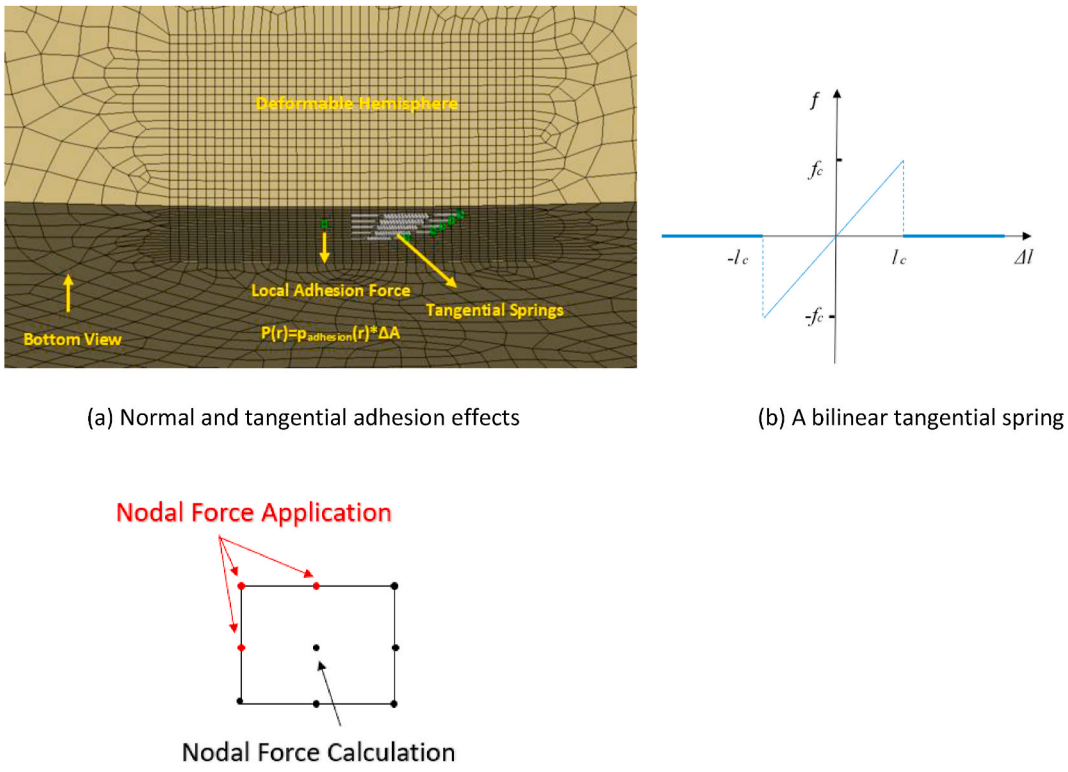

(a) Normal and tangential adhesion effects

(b) A bilinear tangential spring

(c) Nodal force calculation and application on the surface of mesh element in contact.

Fig. 3. Adhesion effects applied at the bottom surface of the sphere.

parameter, l_c, indicates the corresponding limitation of the elongation at breakage, see Fig. 3b. The spring "breaks" when the elongation exceeds l_c, at which instant a surface is created by the energy released from the spring. Additionally, the tangential stress of that local element when each spring breaks equals to the shear strength of the material, S_{sy}. The tangential force is then:

$$kl_c = S_{sy}\Delta A \tag{6}$$

where based on the Tresca failure criterion, $S_{sy} = S_y/2$, and S_y is the yield strength of the material (in the current case, it is that of gold).

By combining equations (5) and (6), the stiffness and limitation of the elongation of each spring can be expressed by:

$$l_c = \frac{2\Delta\gamma}{S_{sy}} \tag{7}$$

$$k = \frac{S_{sy}{}^2\Delta A}{2\Delta\gamma} \tag{8}$$

The material of the sphere is gold [13], properties of which are listed in Table 1. The pull-off force, $F = -F_c$, is the external force needed to part the adhesive contact (i.e., in the negative y-direction), and is given by Refs. [8]:

$$F_c = \frac{3}{2}\Delta\gamma\pi R \tag{9}$$

Table 1
The model geometry, pull off force, and material properties of gold for the model [13].

Parameter	R [mm]	E [GPa]	γ [J/m^2]	S_y [MPa]	ν	S_{sy} [MPa]	F_c [mN]
Au	1	80	0.5	670	0.42	335	0.471

The value of F_c is also provided in Table 1. A small strain hardening of 1% of the elastic modulus is used in the finite element simulation to expedite convergence, which is discussed in the following.

3. Mesh convergence

Fig. 4 shows the model built using the commercial software ANSYS 17.1. A quadratic 3D solid mesh element is used. The model consists of 125,608 mesh elements. The "no separation/penetration" condition is applied to the interface between the deformable hemisphere and the frictionless rigid top plate. That condition means the two contacting surfaces can freely move relative to each other along their interface, but they cannot penetrate each other or be parted. Likewise, frictionless contact conditions are applied to the interface between the deformable hemisphere and the rigid bottom plate. There, however, adhesion takes effect. A Xeon computer with 32 GB of memory using four threads of parallel computing is used to simulate the fretting cases with a maximum duration case of 97 h.

Convergence of the model is mostly influenced by the number of contact elements at the interface between the deformable hemisphere and the rigid bottom plate. The mesh at the interface has been increased successively until the difference between the contact areas at two mesh refinements is smaller than 2%. As shown in Fig. 5, the evolution of the contact area increases with the number of contact elements, subject to an external force that equals to the magnitude of pull-off force. Beyond 100 contact elements the changes in the contact area are slight, so it is determined that 400 contact elements (which is used throughout) are adequate.

By applying the strategy of 400 contact elements, Fig. 6 shows the theoretical contact radius from Eq. (3) and the numerical contact radius from FEA as a function of external forces ranging from $-F_c$ to F_c. The difference between the contact radii from the two different methods is

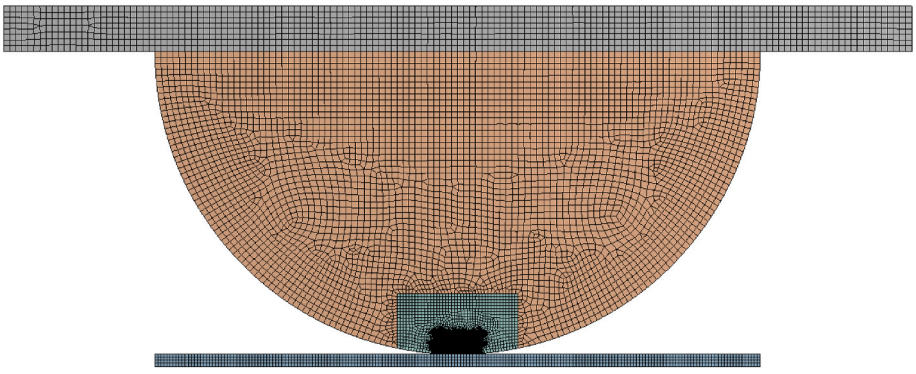

Fig. 4. The mesh model and its refinement in ANSYS 17.1.

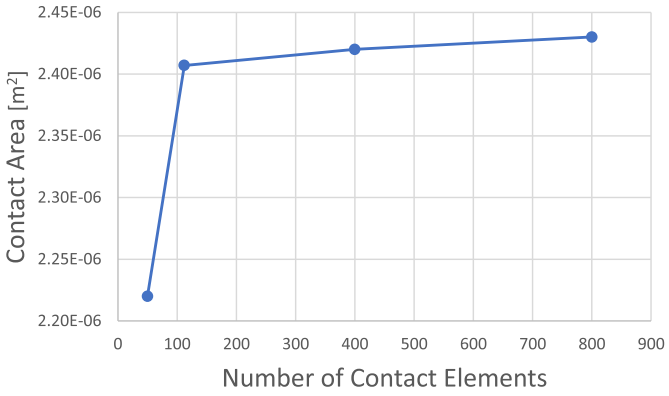

Fig. 5. The evolution of contact area with different number of contact elements.

less than 3%. The good agreement further indicates that the results at the current meshing level have converged and are satisfactorily accurate.

4. Results and discussion

4.1. Results with only normal adhesion

The model is first applied with only normal adhesion, using the classic JKR model and F = 0 (i.e., only adhesion is in effect at the contact). The FEA-based JKR model is applied as shown in Fig. 3a, as described above. Henceforth, if not mentioned specifically otherwise, the additional external normal force is implied to be zero. As given by Equation (4), the pressure is positive when the point is close to the center (the local radius, r, is close to zero). The pressure is negative when the point is close to the edge (the local radius, r, is close to the contact radius, a). At the contact edge, the local radius, r, equals to the contact radius, a, which leads to the theoretical pressure to approach a value of negative infinity (as implied by Eq. (4)). Fig. 7 shows the pressure distributions at the centerline of the contact (x = 0) for both the theoretical JKR model, Eq. (7), and the finite element model built herein. The results are in very good agreement, except at the center point (z = 0) and the edge (z = a). When the point is close to the center, there is a ANSYS programming modeling issue where a nodal force cannot be assigned to a point at the symmetric front plane. This issue leads to the slight difference at or near z = 0. When the point is close to the edge, the theoretical pressure tends to negative infinity. Since the model is discretized by finite mesh elements, the actual value input to the model is also finite, which leads to the difference at or near z = a. In general, however, the pressure distribution shows very good agreement between the theoretical and numerical model, which further verifies the said FEA model.

The von-Mises stress distribution at the interface is shown in Fig. 8. Since the magnitude of the negative pressure at the edge is relatively large (theoretically it tends to infinity, see Eq. (4b)), the von-Mises stress is also relatively large at the contacting edges. The regions in red represent points whose stresses are at or slightly larger than the yield stress (because of the small strain hardening), which means that plasticity takes place there. However, for the most part of the interface, the deformation is elastic. This concludes the verification of the model.

4.2. Results with normal adhesion and tangential resistance

First, the hemisphere is subjected to normal adhesion (as is the case

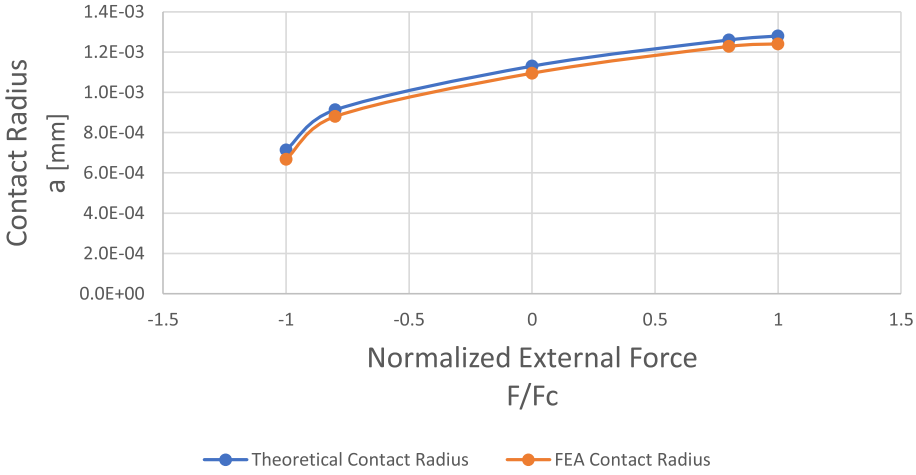

Fig. 6. The contact radii, a, from Eq. (3) theoretically and FEA at different normalized external forces, F/F_c.

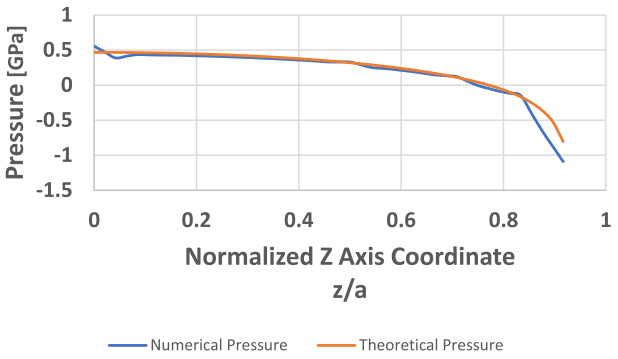

Fig. 7. The pressure distributions at the centerline (x = 0) vs. z for the theoretical JKR and the FEA models for F = 0.

in the JKR model). Then tugging in the tangential direction is imposed (the classical JKR model is not applicable when that happens). Tangential resistance is established by the said interfacial bilinear springs as discussed previously in Section 2. In this section, the external force is either F = 0 or F=F_c. The detachment of the contact element is achieved by the "breakage" of the spring, i.e., its elongation surpassed l_c (see Eq. (7)). When that happens, the work that is done upon the spring (i.e. strain energy stored) equals to the surface free energy multiplied by the area of the mesh element. The force that the spring exerts equals to the shear strength multiplied by the area of the mesh element. Due to the oscillatory behavior of the fretting motion, the elongation of spring will start to decrease after the hemisphere reaches the rightmost or leftmost position (position B and D in Fig. 2). After breakage, when the spring elongation returns to the range (-lc,lc) (Fig. 3b), reattachment of the spring takes place.

The nominal tangential displacement, δ, is defined as the transverse displacement applied to the top surface of the hemisphere in the X-direction. Fig. 9 shows a typical trend of the evolution of the tangential force with the increase of the nominal tangential displacement, δ. For the pure elastic case, with the increase of δ, the spring forces at the interface increase linearly without breakage. Once one of the springs length reaches the breakage limitation, the spring breaks, which represents the detachment of the local contacting elements. That reduces the number of springs that support the tangential force, causing the force that each spring needs to hold to increase. That generates an avalanche of springs breakage.

However, when plasticity is introduced into the model, as the von-Mises stress reaches the yield strength of the material, the model structure-wise becomes more flexible. The relative displacement at the interface is larger, which allows the springs not to reach the breakage limitation all at the same time. In this situation, some springs break first, while others break later, which makes the springs breakage more gradual. Since the springs do not break simultaneously, the largest tangential traction that the model generates is somewhat smaller than that of the purely elastic case. As shown in Fig. 9, although the breakage is gradual, the breakage in the elasto-plastic case is still avalanching only when it passes the largest tangential force the springs can support. Assume that all springs break at the same instant at the interface. According to Equations (7) and (8), the force that each spring generates at breakage limitation, f_c, is:

$$f_c = kl_c = S_{sy}\Delta A \tag{10}$$

The total number of springs at the interface is:

$$N = \frac{\pi a^2}{\Delta A} \tag{11}$$

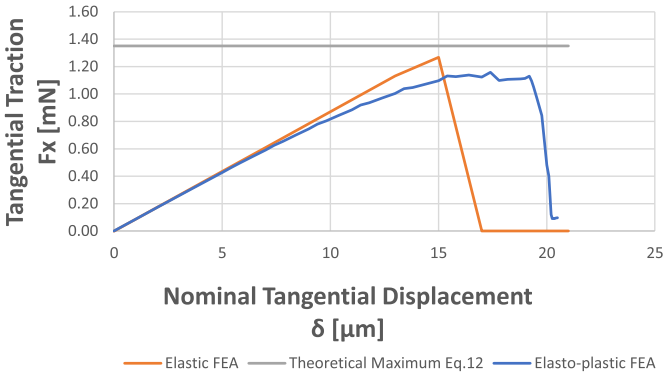

Fig. 9. The evolution of the tangential force with respect to the nominal tangential displacement during unidirectional sliding.

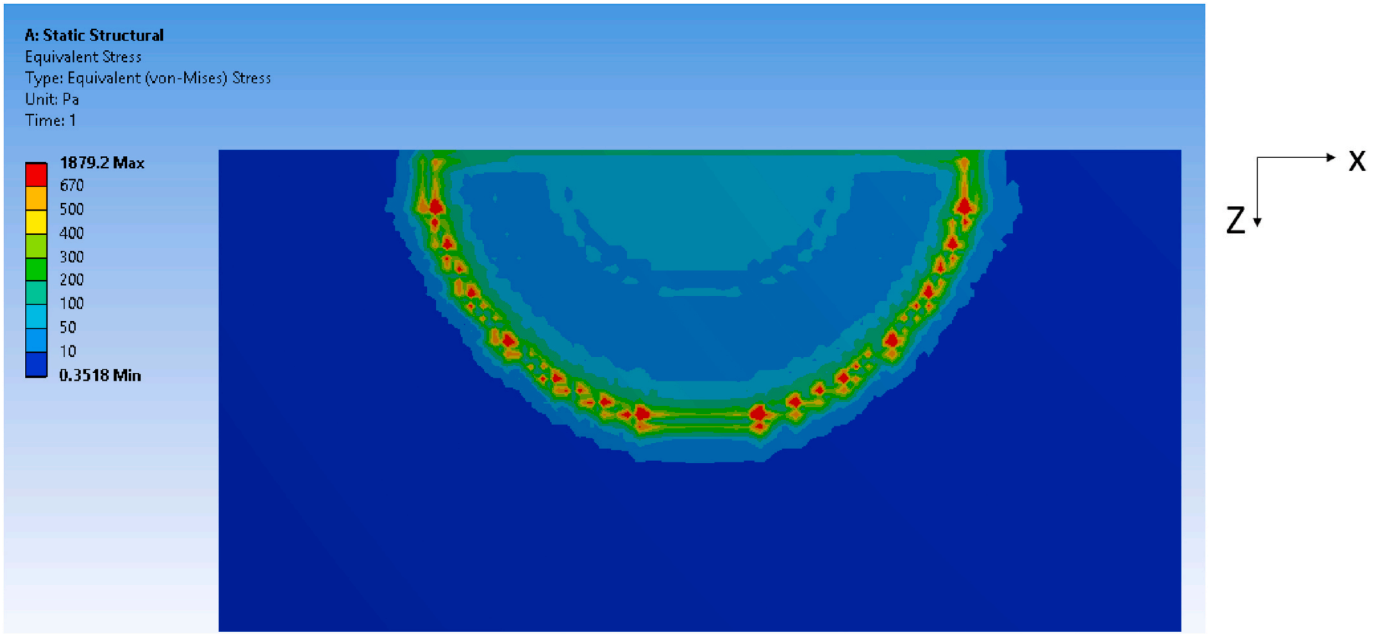

Fig. 8. Von-Mises distribution for normal direction model.

Then, the total maximum tangential traction that the springs can generate is:

$$F_{x,\max} = Nf_c = S_{sy}\pi a^2 \tag{12}$$

The maximum tangential force, $F_{x,max}$, at zero normal external force based on Eq. (12) is also shown in Fig. 9. It is close to the numerical $F_{x,max}$ in the elastic and elasto-plastic case, which further corroborates the model. Additionally, the theoretical $F_{x,max}$ should be a physical value for a certain external normal force. In other words, $F_{x,max}$ should not be influenced by the mesh size, the stiffness, or the breakage limitation of the springs. As implied by Eq. (12), this is indeed true for the current model, as it is apparent from Fig. 9.

The tangential resistant traction also affects the distribution of the von-Mises stress. Fig. 10 shows the distribution of von-Mises stress at the interface just before the breakage of the springs at the interface. The regions in red represent elements where the von-Mises stress is larger than the yield strength of gold (670 MPa). As seen, the von-Mises stress is large over a significant interfacial area indicating plasticity. That is now examined via the equivalent plastic strain, shown in Fig. 11.

Since the tangential resistant traction increases the von-Mises stress at and near the contacting edges, larger equivalent plastic strains are present there, too. Fig. 11 shows the distribution of the equivalent plastic strains at the interface after one cycle of fretting motion. The magnitude of the tangential displacement is 20 nm that guarantees to be large enough so that the hemisphere passes the position where all the springs break. While the classical normal direction JKR model only generates plasticity within a tiny part at the contacting edges, the combination of the normal and tangential direction adhesion model generates plastic strains that nearly encompass the entire interface. This behavior occurs also when the external normal load takes any value in the range between $-F_c$ and F_c. Thus, normal adhesion and tangential resistance produce an interface that is predominantly in the elasto-plastic state.

When the fretting cyclic tangential displacement is applied to the top surface of the sphere, there are two types of fretting loops. On the one hand, when the maximum nominal displacement is small (less than 15 nm as shown in Fig. 9), the springs do not break, and the evolution of the tangential force does not produce a large energy loss. On the other hand, when the maximum nominal displacement is large (20 nm, also see Fig. 9) the springs break, and the evolution of the tangential force does produce a large energy loss. This is discussed next.

Fig. 12 shows the evolution of the tangential force at an external normal force $F=F_c$ for two cycles of fretting motion with a relatively small fretting displacement magnitude of 15 nm. Since no spring ever breaks, the shape of the fretting loop is similar to that in full stick conditions, as described in Ref. [21]. The small energy loss is due to the dissipation of plastic strain energy. An effective COF based on the definition from Green [23] is introduced here:

$$\mu_{eff} = \frac{U_{net}}{\int F_y dx} = \frac{\int F_x dx}{\int F_y dx} \tag{13}$$

where U_{net} represents the net energy loss during the fretting cycles, and F_y represents the normal external force. U_{net} is calculated by numerical quadrature. The calculated COF is $\mu_{eff} = 0.23$ for the case of 15 nm oscillation amplitude.

At a relatively larger fretting oscillation amplitude, say of 20 nm, the springs do break, and the evolution of the tangential force generates large energy losses. Fig. 13 shows the evolution of the tangential force also at an external normal force of $F=F_c$ for two cycle of fretting motions with the said larger fretting oscillation amplitude of 20 nm. At the very beginning, the hemisphere moves in the positive X direction. The tangential force increases with the nominal displacement applied to the top surface of the hemisphere. After the springs break at the interface, the tangential force decreases sharply to a very small value but not to zero due to the elastic resistance caused by the indentation, which is restored. As the hemisphere turns back in the negative X direction, the lengths of the springs drop and tangential adhesion is reinstated, causing the reattachment of the two surfaces. Thus, the tangential forces increase somewhat with the retracted motion. As the hemisphere approaches the original center point, some of the springs change status from stretched to compressed, and thus the tangential forces decrease again. For the hysteretic loop shown in Fig. 13, the calculated COF is $\mu_{eff} = 0.70$ for the case of 20 nm oscillation amplitude.

Note that the fretting loop in Fig. 13 is not similar to that in gross slip conditions for models without adhesion [24]. The variation is caused by the spring's detachment and reattachment mechanism used in the current model. Herein, there is no application of a "coefficient of friction;" adhesive detachment or reattachment happens only when the elongation is out of or returns to the range $(-l_c, l_c)$, respectively. In other models that apply some arbitrary "constant" COF, the friction force that is generated [24], along with the fretting loops, correspond only to those arbitrarily postulated COFs.

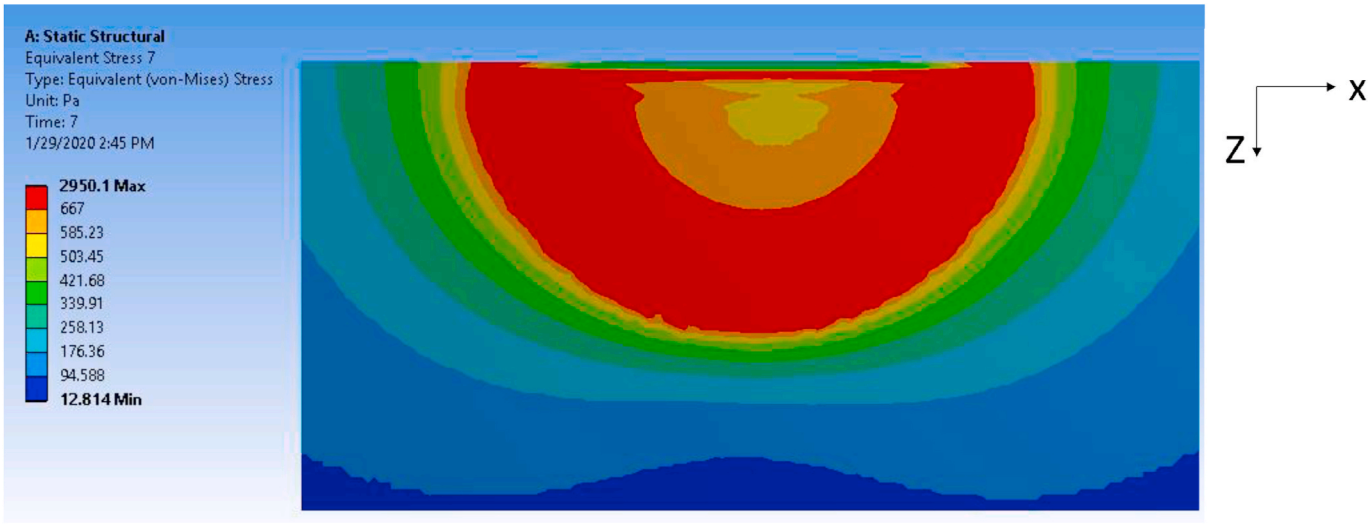

Fig. 10. The distribution of the von-Mises stress of the hemisphere at the interface (y = 0) at the breakage of the springs for the normal and tangential directions adhesion after one cycle of fretting motion. Motion is in the positive X direction, while Z is the transverse direction, F = 0, δ = 20 nm.

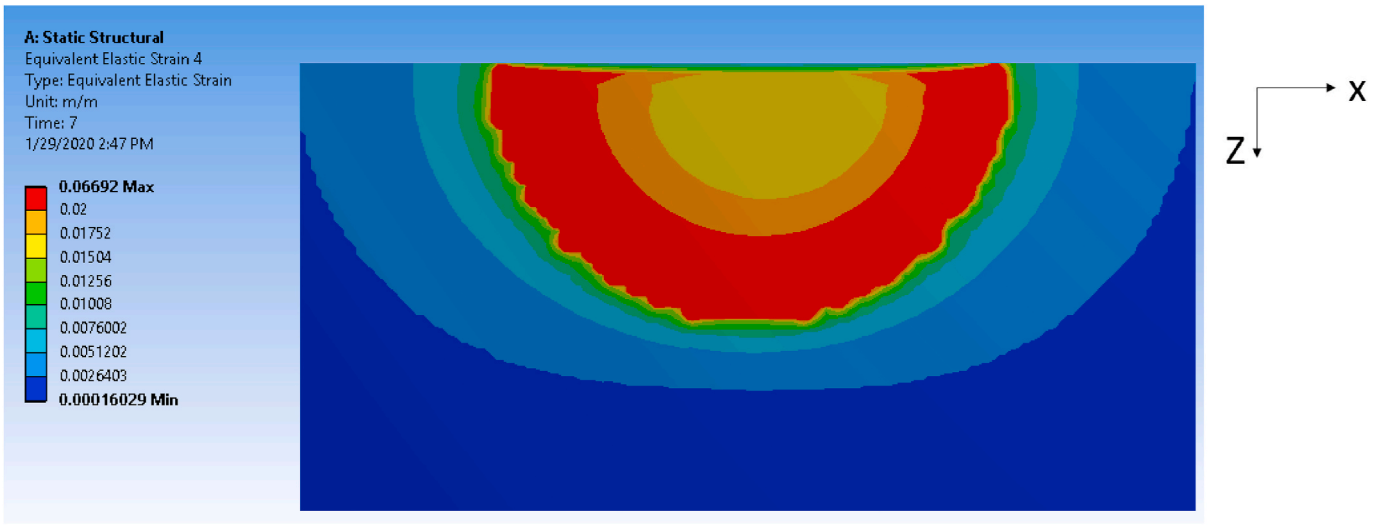

Fig. 11. The distribution of the equivalent plastic strain after one cycle of fretting motion including normal and tangential directions adhesion effects.

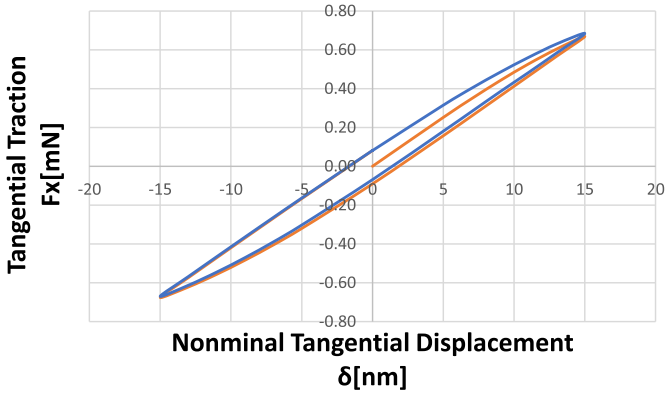

Fig. 12. The evolution of the tangential force at Fc external normal force for two cycle of fretting motion with a smaller fretting displacement magnitude of 15 nm (1st cycle = orange, 2nd cycle = blue). (For interpretation of the references to colour in this figure legend, the reader is referred to the Web version of this article.)

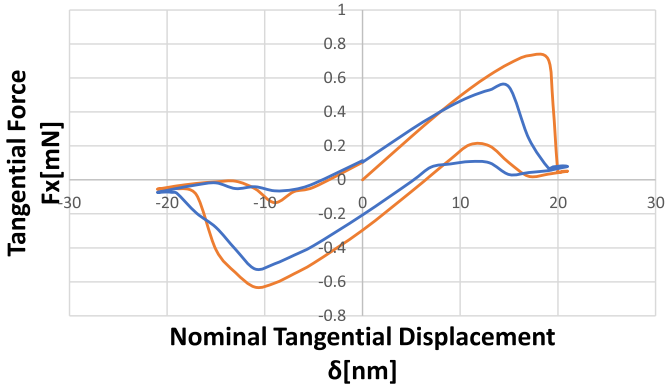

Fig. 13. The evolution of the tangential force at Fc external normal force for two cycles of fretting motion with a larger fretting displacement magnitude of 20 nm (1st cycle = orange, 2nd cycle = blue). (For interpretation of the references to colour in this figure legend, the reader is referred to the Web version of this article.)

4.3. Comparisons between adhesion and non-adhesion models

To understand further the mechanism of the adhesion model used in this work, the distribution of the von-Mises stresses, the equivalent plastic strains, and the evolution of the tangential resistant forces are compared now using three different models for an oscillation amplitude of 15 nm (no spring breakage, i.e., adhesion is steadfastly in effect):

Model A. This is precisely the model described throughout this work: The model includes JKR adhesion in the normal direction, but with tangential resistance by means of bilinear springs.

Model B. The model is with JKR adhesion in the normal direction and frictional contact in the tangential direction. The coefficient of friction (COF), however, is set sufficiently large (COF = 10) to cause and maintain full stick conditions at all times.

Model C. The model is a pure Hertizan contact model in the normal direction and a frictional contact in the tangential direction. Again, the COF is set sufficiently large to cause and maintain full stick condition at all times. While no adhesion is applied here, the normal external force is increased to maintain the same contact area as those in models A and B.

As indicated the COF in frictional contact is set to be large enough to maintain full stick in model B and C, but in model A, no COF is applied at all. In model A adhesion resistance to sliding is done by the tangential bilinear springs until they avalanching break. The results just right before that breakage (i.e., contact condition change from full stick to gross slip) are compared herein. The input of the nominal tangential displacement on the top surface of the hemisphere are maintained the same for all three models. Model C with the same external normal load is not considered, because its contact area is tiny, and the results are trivial.

Fig. 14 shows the distribution of the von-Mises stress at the bottom interface of the hemisphere for the three models. For Model A, the largest von-Mises stress is located at the edges due to the infinite normal pressure as implied by the JKR model. For Model B, the largest von-Mises is also located at the edges. The stresses in Model B are larger at the center compared to A, because of the full stick condition, as effectively model B possesses structurally a higher stiffness than the bilinear springs (in Model A). It is thus capable of transmitting an increased tangential load under the same tangential displacement input. For Model C, the stress distribution is typical of a full stick Hertzian contact. The region in red is where the von-Mises stress reaches the yield strength to indicate plasticity. The area of plasticity in Model C is considerably larger than those in models A and B.

Although the distributions of the von-Mises stress at the bottom surface of the hemisphere are different in the three models, the

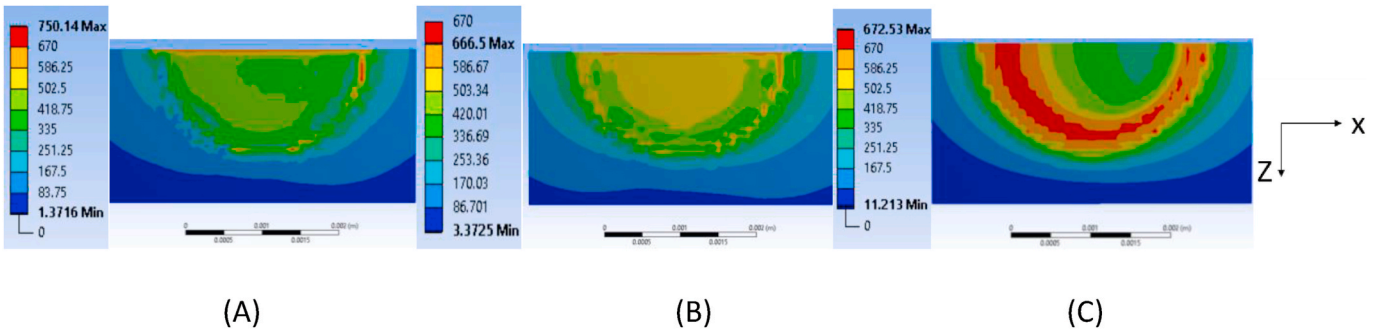

Fig. 14. Bottom view. The distribution of the von-Mises stress at the bottom interface of the hemisphere (y = 0) having the same tangential displacement to the right (but just before the breakage of springs in model (A) for all three models.

distributions are somewhat similar for the front surface, i.e., the XY plane where at z = 0 (see definitions in Fig. 1). Fig. 15 shows the distributions of the von-Mises stress under the same condition for the front view for the three models. The large von-Mises stresses are located at the region near the interface, and the von-Mises stresses spread to a larger area to the "left) side than that on the "right," because the direction of the (reactive) tangential force is in the negative x direction (i.e., to the "left") when the hemisphere is forced in the positive x direction (or, to the "right").

Fig. 16 shows the distribution of the equivalent plastic strains at the bottom of the sphere for three models. For Model A, the plastic deformation is mainly due to the JKR model producing infinite pressure at the contact edges. For Model B, since the tangential load is larger (as seen in Fig. 15), the plastic strain is therefore larger than model A. For Model C, plasticity (i.e., the von-Mises stress reaching the yield strength) does not show up after normal contact, since there is no JKR pressure. During the fretting motion, plastic strain appears at the very beginning, at point A_1 (see Fig. 2) for Models A and B, while the plastic strain appears later between points A_1 and B_1 for Model C. The later appearance of plastic strain in Model C causes a smaller spread region than the other two.

Fig. 17 shows the tangential force evolutions during one cycle of fretting loading for the three models (recall that all models have a smaller oscillation amplitude of 15 nm). All three tangential force evolutions are typical for fretting loop of full stick conditions. However, the slopes of the fretting loop are different. For model A, the elastic bilinear springs at the interface have the least effective stiffness. The large plastic deformation at the contact edges of JKR model also decreases the tangential resistance. Thus, it has the smallest slope or inclination. For model C, it is in a full stick condition with no JKR pressure, which produces the largest effective structural stiffness. Thus, it has the largest slope. Model B is a transition model between models A and C, where the structural stiffness of model B is in between.

In conclusion, up to the point where the bilinear spring in the adhesion model A do not break, that model exhibits von-Mises stresses distribution, plastic strain distributions (see Fig. 16), and fretting loops (see Fig. 17) similar to the full stick contact model C. The plastic damage is more concentrated in this model A due to the infinite JKR pressure. The contact system is less stiff in this model A due to the smaller tangential resistance of the interfacial bilinear springs.

5. Conclusion

This work builds a comprehensive adhesion model that incorporates adhesive tangential resisting traction between a deformable hemisphere and a rigid plate. The normal direction load is based on the classical JKR model. However, the tangential adhesive resistance is based on the definition of shear strength and surface free energy. The model is built using the FEA commercial code ANSYS, with bilinear elastic springs and nodal forces applied at the interface. The material for the deformable hemisphere is gold. Several conclusions are drawn:

1. The robust adhesion model in the tangential direction is not influenced by the mesh and the spring settings.
2. The detachment of the adhesive bond of the two contacting surfaces is achieved by the breakage of the bilinear springs at the interface. The breakage of the springs is avalanching in both elastic and plastic conditions, but is somewhat more gradual with the latter. When the two surfaces are about to detach, the vast part of the contact region deforms plastically.
3. There are two types of fretting loop depending on the magnitude of the oscillatory tangential displacement. At small fretting amplitudes, the fretting loop is similar to that of full stick conditions (as if the contacting model has an interfacial friction force that is exceedingly large). At large fretting amplitudes, the fretting loop generates large energy losses, while the fretting loop is dissimilar than those created by gross slip conditions.
4. The adhesion model in this work exhibits similar patterns in von-Mises stress distribution, plastic strains distribution, and fretting

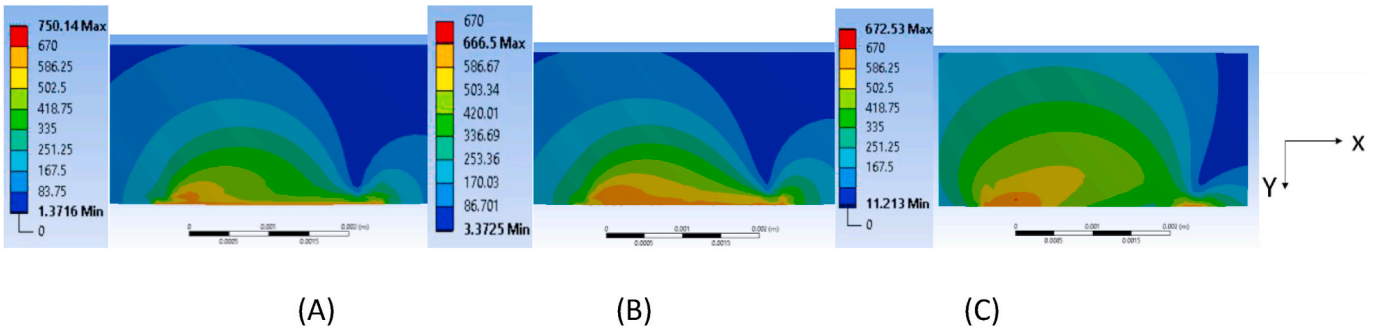

Fig. 15. Front view. The distribution of the von-Mises stress at the front surface (XY plane and z = 0) of the hemisphere having the same tangential displacement to the right (but just before the breakage of springs in model A) for all three models.

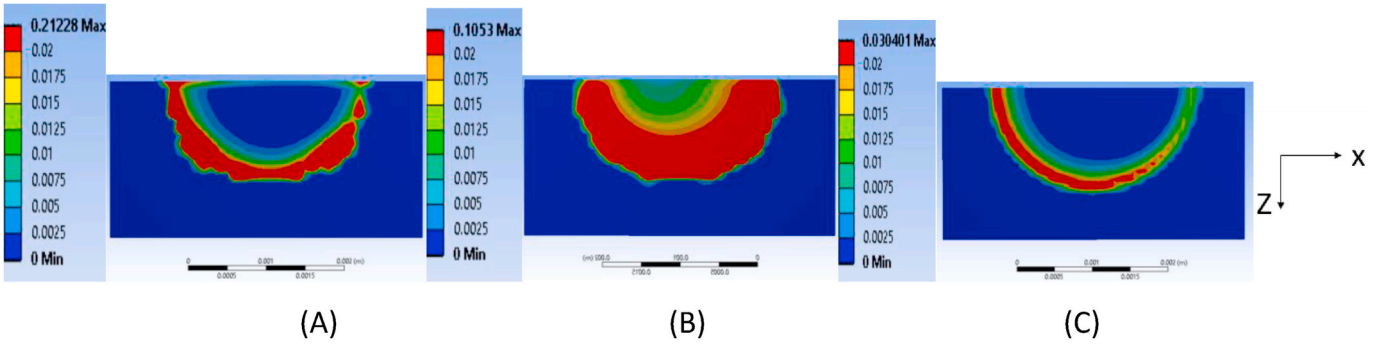

Fig. 16. The distribution of the equivalent plastic strains at the bottom of the hemisphere at the same tangential displacement to the right (before the breakage of springs in model (A) for three models.

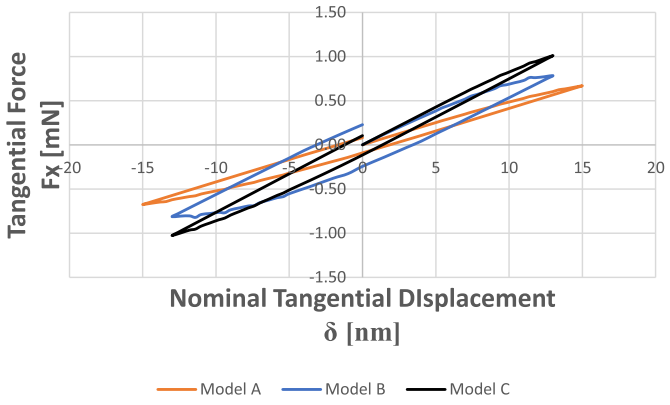

Fig. 17. The evolution of the tangential force during one cycle of fretting load for three models.

loops as the full stick contact models up to the point of breakage. The plastic strain is larger in JKR pressure than that in pure Hertzian model. The contact system is less stiff in this model due to the tangential resisting springs added at the interface.

CRediT authorship contribution statement

Huaidong Yang: Conceptualization, Methodology, Software, Writing - original draft, Data curation. **Itzhak Green:** Conceptualization, Methodology, Writing - review & editing.

Declaration of competing interest

The authors declare that they have no known competing financial interests or personal relationships that could have appeared to influence the work reported in this paper.

Acknowledgement

This research is supported by the Department of Energy under Project 2506U87, Award RH452. This support is gratefully acknowledged.

References

[1] Olsson H, Åström KJ, De Wit CC, Gäfvert M, Lischinsky P. Friction models and friction compensation. Eur J Contr 1998;4(3):176–95.
[2] Johnson K. Adhesion and friction between a smooth elastic spherical asperity and a plane surface. Proc. the Royal Soc. London A: Math. Phys. Eng. Sci. 1997;453:163–79.
[3] Bowden FP, Bowden FP, Tabor D. The friction and lubrication of solids. Oxford university press; 2001.
[4] Keller D. Adhesion between solid metals. Wear 1963;6(5):353–65.
[5] Buckley DH. The metal-to-metal interface and its effect on adhesion and friction. Plenary and invited lectures. Elsevier; 1977. p. 37–54.
[6] Burwell J, Strang C. On the empirical law of adhesive wear. J Appl Phys 1952;23(1):18–28.
[7] Dessureautt M, Spelt J. Observations of fatigue crack initiation and propagation in an epoxy adhesive. Int J Adhesion Adhes 1997;17(3):183–95.
[8] Johnson KL, Kendall K, Roberts A. Surface energy and the contact of elastic solids. Proc. Royal Soc. London. A. Math. Phys. Sci. 1971;324(1558):301–13.
[9] Derjaguin BV, Muller VM, Toporov YP. Effect of contact deformations on the adhesion of particles. J Colloid Interface Sci 1975;53(2):314–26.
[10] Tabor D. In: Surface forces and surface interactions," Plenary and invited lectures. Elsevier; 1977. p. 3–14.
[11] Maugis D. Adhesion of spheres: the JKR-DMT transition using a Dugdale model. J Colloid Interface Sci 1992;150(1):243–69.
[12] Li L, Song W, Xu M, Ovcharenko A, Zhang G. Atomistic insights into the loading–unloading of an adhesive contact: a rigid sphere indenting a copper substrate. Comput Mater Sci 2015;98:105–11.
[13] Du Y, Chen L, McGruer NE, Adams GG, Etsion I. A finite element model of loading and unloading of an asperity contact with adhesion and plasticity. J Colloid Interface Sci 2007;312(2):522–8.
[14] Yoshizawa H, Chen YL, Israelachvili J. Fundamental mechanisms of interfacial friction. 1. Relation between adhesion and friction. J Phys Chem 1993;97(16):4128–40.
[15] Binnig G, Quate CF, Gerber C. Atomic force microscope. Phys Rev Lett 1986;56(9):930.
[16] Carpick RW, Salmeron M. Scratching the surface: fundamental investigations of tribology with atomic force microscopy. Chem Rev 1997;97(4):1163–94.
[17] Lantz M, O'shea S, Welland M, Johnson K. Atomic-force-microscope study of contact area and friction on NbSe 2. Phys Rev B 1997;55(16):10776.
[18] Wei Z, Wang C, Bai C. Investigation of nanoscale frictional contact by friction force microscopy. Langmuir 2001;17(13):3945–51.
[19] Popov VL, Lyashenko IA, Filippov AE. Influence of tangential displacement on the adhesion strength of a contact between a parabolic profile and an elastic half-space. Royal Soc. Open Sci. 2017;4(8):161010.
[20] Yang H, Green I. Fretting wear modeling of cylindrical line contact in plane-strain borne by the finite element method. J Appl Mech 2019;86(6).
[21] Yang H, Green I. Analysis of displacement-controlled fretting between a hemisphere and a flat block in elasto-plastic contacts. J Tribol 2019;141(3):031401.
[22] Knothe K. Contact mechanics and friction: physical principles and applications. London, England: SAGE Publications Sage UK; 2011.
[23] Green I. An elastic-plastic finite element analysis of two interfering hemispheres sliding in frictionless contact. Physical Science International Journal 2018:1–34.
[24] Yang H, Green I. Analysis of displacement-controlled fretting between a hemisphere and a flat block in elasto-plastic contacts. J Tribol 2019;141(3).